Nanotechnology **22** (2011) 505104 (9pp) doi:10.1088/0957-4484/22/50/505104

Surface-biofunctionalized multicore/shell CdTe@SiO_2 composite particles for immunofluorescence assay

Lihong Jing[1], Yilin Li[1], Ke Ding[1], Ruirui Qiao[1], Andrey L Rogach[2] and Mingyuan Gao[1,3]

[1] Institute of Chemistry, Chinese Academy of Sciences, Bei Yi Jie 2, Zhong Guan Cun, Beijing 100190, People's Republic of China
[2] Department of Physics and Materials Science and Centre for Functional Photonics, City University of Hong Kong, Tat Chee Avenue, Kowloon, Hong Kong

E-mail: gaomy@iccas.ac.cn

Received 21 September 2011, in final form 13 October 2011
Published 23 November 2011
Online at stacks.iop.org/Nano/22/505104

Abstract
Strongly fluorescent multicore/shell structured CdTe@SiO_2 composite particles of ~50 nm were synthesized via the reverse microemulsion method by using CdTe quantum dots co-stabilized by thioglycolic acid and thioglycerol. The optical stability of the CdTe@SiO_2 composite particles in a wide pH range, under prolonged UV irradiation in pure water, or in different types of physiological buffers was systematically investigated. Towards immunofluorescence assay, both poly(ethylene glycol) (PEG) and carboxyl residues were simultaneously grafted on the surface of the silanol-terminated CdTe@SiO_2 composite particles upon further reactions with silane reagents bearing a PEG segment and carboxyl group, respectively, in order to suppress the nonspecific interactions of the silica particles with proteins and meanwhile introduce reactive moieties to the fluorescent particles. Agarose gel electrophoresis, dynamic light scattering and conventional optical spectroscopy were combined to investigate the effectiveness of the surface modifications. Via the surface carboxyl residue, various antibodies were covalently conjugated to the fluorescent particles and the resultant fluorescent probes were used in detecting cancer cells through both direct fluorescent antibody and indirect fluorescent antibody assays, respectively.

S Online supplementary data available from stacks.iop.org/Nano/22/505104/mmedia

(Some figures may appear in colour only in the online journal)

1. Introduction

Molecular probes based on fluorescent quantum dots (QDs) are attracting increasing attention owing to their remarkable optical properties governed by the quantum confinement effect [1–3]. Spectral features of QDs such as broad excitation range, narrow and symmetric emission, large molar extinction coefficients, high fluorescence quantum yields (QY) and size-dependent emission tunable over a broad spectral range from UV to the near-IR are considered advantageous for their applications in both bioanalysis [4–7] and bioimaging [2, 3, 8–11]. Over the past two decades, significant progress has been achieved in the colloidal synthesis and surface engineering of QDs [12]. However, due to the dynamic nature of the QD surface capped by organic ligands, the strong surface defect-dependent fluorescence [13–15], as well as the release of toxic metal ions upon photooxidation [16], the use of 'bare' QDs still faces inherent disadvantages in bioapplications.

Encapsulation of QDs by silica has been considered as an effective approach for overcoming these drawbacks [17–33]. Silica encapsulation of QDs can typically be realized by two approaches, i.e. the Stöber process and reverse microemulsion (water-in-oil) method. In the former approach, a pre-coating of QDs using amino- or mercapto-derived silane primers

[3] Author to whom any correspondence should be addressed.

is typically required in order to make the QD surface vitreophilic prior to the silica coating [18, 21–23], while the latter approach does not necessarily require such a pre-coating procedure in encapsulating both hydrophilic [27] and hydrophobic QDs [26, 29]. Most importantly the latter method offers the possibility for producing 40–100 nm QD/silica composite particles which are greatly desirable for various bioapplications. But no matter by which approaches, a drastic decrease in the fluorescence QY of the QDs encapsulated is a common problem. In addition, effective controls over the number of the incorporated QDs, size and size distribution of the resultant composite particles remain difficult [21, 29, 30].

Recently, important breakthroughs in synthesizing highly fluorescent silica particles with controllable composite structures have been achieved in the reverse microemulsion method [27, 28, 34]. A typical microemulsion system is comprised of cyclohexane, Triton X-100 (t-octylphenoxypolyethoxyethanol), n-hexanol, ammonia and CdTe QDs stabilized by various types of thiol molecules [27, 28]. Upon the hydrolysis and the following condensation of tetraethyl orthosilicate (TEOS) in the water microdroplets, highly fluorescent and mono-dispersed CdTe@SiO_2 composite particles of 45–109 nm can be obtained [27, 28]. Moreover, the resultant composite particles exhibit a unique core/shell structure with single CdTe QD cores. Systematic investigations reveal that the electrostatic repulsion between the negatively charged CdTe QDs mediated by the negatively charged silica intermediates formed upon the hydrolysis of TEOS is responsible for such core/shell structures [27]. In this mechanism, either by reducing the negative surface potential through incubating the CdTe QDs in ammoniacal solution [34], or introducing polycations into the reaction system to reduce the electrostatic repulsions between CdTe QDs [27], the number of CdTe QDs encapsulated can effectively be increased. Especially by the former approach, multicore/shell CdTe@SiO_2 composite particles with a fluorescence QY of 47% are successfully obtained. Nevertheless, to further explore their applications in bioassays such as cancer cell labeling, the nonspecific interactions between the silica particles and cells have to be overcome, and the binding specificity needs to be achieved with the aid of target-specific bioligands, which remains challenging [35–38].

Herein we report our investigations on the surface anti-biofouling coating and carboxyl derivatization for the multicore/shell CdTe@SiO_2 composite particles for achieving EGFR (epidermal growth factor receptor)-specific molecular probes. The anti-biofouling coating is expected to minimize the nonspecific adsorption of immunoglobulin G (IgG) while the surface reactive carboxyl can be used for further covalently coupling bioligands of interest to form robust fluorescence molecular probes. Following these ideas, both poly(ethylene glycol) (PEG) and carboxyl residues were simultaneously grafted onto the silanol-terminated surface of the CdTe@SiO_2 composite particles by using suitable silane reagents bearing PEG segments and carboxyl groups, respectively. Based on the optimization of the surface functional coatings, goat anti-human immunoglobulin G (GaHIgG) antibody was conjugated to the CdTe@SiO_2 composite particles via the amidation reaction and the resultant nanoprobes were used in detecting the UM-SCC-22B human head and neck squamous cell carcinoma cell line cells via the indirect fluorescent antibody assay (IFA). For comparison, human anti-EGFR monoclonal antibody (anti-EGFR-mAb) was also labeled by the highly fluorescent CdTe@SiO_2 particles and the resultant conjugates were used in detecting the same cell line via the direct fluorescent antibody assay (DFA).

2. Experimental details

2.1. Chemicals

Methoxy(polyethyleneoxy)propyltrimethoxysilane (PEOS; Gelest Inc., 90%), carboxyethylsilanetriol sodium salt (CES; Gelest Inc., 25% in water), *N*-hydroxysulfosuccinimide sodium salt (Sulfo-NHS; Sigma-Aldrich, 98.5%+), *N*-(3-dimethylaminopropyl)-*N*′-ethylcarbodiimide (EDC; Sigma-Aldrich, purum, ⩾97.0%), agarose (Biowest Agarose), Tris (Amresco, 99.9%), Dulbecco's Modified Eagle Medium (DMEM) (M&C Gene Technology), Minimum Essential Medium (MEM) (Hyclone) and Roswell Park Memorial Institute Medium 1640 (RPMI 1640) (Solarbio) were used as received. Phosphate buffer (PB) and phosphate buffered saline (PBS) were prepared with Milli-*Q* water. The UM-SCC-22B human head and neck squamous cell carcinoma cell line was a gift from Peking University. Human anti-epidermal growth factor receptor monoclonal antibody (anti-EGFR-mAb) was purchased from Baitai Biological Pharmaceutical Corporation and used after dialysis. Goat anti-human immunoglobulin G (GaHIgG) was purchased from Beijing Solarbio Science & Technology Co.

2.2. Synthesis of CdTe QDs

Aqueous CdTe QDs co-stabilized by thioglycerol (TG) and thioglycolic acid (TGA) were synthesized, upon the reaction between Cd^{2+} and H_2Te, according to the method reported previously [39–42]. In difference, the initial pH of the precursor solution was set to 12 and the ratio of Cd:HSR was adjusted from 1:2.4 to 1:1.3.

2.3. Synthesis of multicore/shell CdTe@SiO_2 composite particles

The highly fluorescent multicore/shell CdTe@SiO_2 composite particles were prepared by the reverse microemulsion method according to our previous publications [27, 28, 34]. In brief, 15 ml of cyclohexane, 1.5 ml of n-hexanol, 2.25 ml of Triton X-100, 20 μl of aqueous solution of PDDA (12.8 mol l^{-1}) and 1 ml of the as-prepared CdTe QD solution containing 0.45 wt% ammonia and 15.9×10^{-3} mol l^{-1} NaOH were first mixed in a flask under vigorous stirring for 40 min. After 100 μl of TEOS was introduced, the flask was sealed and kept under stirring in the dark at room temperature for three days. Isopropanol was used to terminate the reaction and the resultant precipitate of CdTe@SiO_2 composite particles was washed in sequence with ethanol and water for three cycles and centrifugation was employed to collect the particles in between.

2.4. Surface PEG modification and carboxyl derivatization

Typically, 20 mg purified CdTe@SiO_2 composite particles were mixed with CES and PEOS in 1 ml phosphate buffer (PB) (10 mM, pH 7.4) by molar ratios of 1:0:0, 1:264 000:143 250, 1:66 000:143 250 and 1:66 000:35 813. The reactions were allowed to proceed for 24 h. The particles were collected by centrifugation, and washed by PB for three times. The resultant particles finally obtained were dispersed in PB for the following experiments and denoted as sample **A**, sample **B**, sample **C** and sample **D**, respectively.

2.5. Covalent conjugation of IgG to CdTe@SiO_2 composite particles

Samples **B**–**D** were mixed with EDC and Sulfo-NHS (molar ratio of CdTe@SiO_2:EDC:Sulfo-NHS = 1:10 000:25 000) in aqueous solution under gentle stirring for 20 min and then GaHIgG was introduced by weight ratio of CdTe@SiO_2:GaHIgG = 1:0.1, followed by addition of PB. The mixture in 1 × PB was incubated at 37 °C for 4 h. The final products of the conjugation reaction, denoted as **B**–GaHIgG, **C**–GaHIgG and **D**–GaHIgG, respectively, were purified by centrifugation and washed for three cycles by 1 × PB to remove EDC/Sulfo-NHS and unreacted GaHIgG molecules. In parallel, the above experiments were repeated but in the absence of EDC/Sulfo-NHS by using samples **A**–**D**. After the same purification process, the resultant samples were denoted as **A** + GaHIgG, **B** + GaHIgG, **C** + GaHIgG and **D** + GaHIgG, respectively. In addition, **D**–(anti-EGFR-mAb) conjugates were also prepared according to the procedures mentioned above.

2.6. Immunofluorescence labeling of cancer cells

Both indirect fluorescent antibody and direct fluorescent antibody assays were adopted for detecting UM-SCC-22B human head and neck squamous cell carcinoma cells fixed by paraformaldehyde. In the IFA process, the fixed UM-SCC-22B cells were firstly incubated with 1% BSA (1 ml) in a 35 mm confocal dish with a glass bottom for 1 h at 37 °C and then 100 μl of 0.2 mg ml^{-1} anti-EGFR-mAb was introduced to combine with cell-surface-expressed EGFR after excess BSA was removed. This incubation process lasted for 18 h at 4 °C. The resultant cells were washed with PBS buffer and then incubated with 100 μl of 1 mg ml^{-1} CdTe@SiO_2–GaHIgG conjugates or 100 μl of 1 mg ml^{-1} corresponding mother CdTe@SiO_2 particles at 37 °C for 1 h in 1 × PB. As an additional control experiment, an equal amount of the CdTe@SiO_2-GaHIgG conjugates was also incubated with the fixed UM-SCC-22B cells that were not pre-treated by anti-EGFR-mAb. In the DFA process, the fixed UM-SCC-22B cells were firstly incubated with 1% BSA (1 ml) at 37 °C for 1 h. After being washed with PBS buffer, the cells were then incubated with 100 μl of 1 mg ml^{-1} CdTe@SiO_2–(anti-EGFR-mAb) conjugates for 18 h at 4 °C. For control experiments, the CdTe@SiO_2–(anti-EGFR-mAb) conjugates were replaced by either CdTe@SiO_2–(rabbit IgG) or the mother CdTe@SiO_2 particles with the remaining binding process being unchanged.

2.7. Characterizations

Fluorescence and UV–vis absorption spectra were recorded with a Cary Eclipse fluorescence spectrophotometer and a Cary50 UV–vis spectrophotometer, respectively. TEM images were recorded with a JEM-100CXII microscope operating at an accelerating voltage of 100 kV. SEM images were obtained on a Hitachi S-4800 microscope. Dynamic light scattering (DLS) measurements were carried our at 298.0 K with a Nano ZS (Malvern) equipped with a solid state He–Ne (λ = 633 nm) for measuring the hydrodynamic size and zeta potential. An FV 1000 confocal laser scanning microscope was used to acquire both confocal fluorescence (excited at 405 nm) and transmitted light differential interference contrast images (by 488 nm laser line) of the cell samples. Agarose gel electrophoresis experiments were carried out by using 0.5% agarose gel cast in tris-borate buffer (1 × TB, pH = 8.0). Typically 15 μl aqueous dispersion of the CdTe@SiO_2 composite particles was mixed with 5 μl glycerol in TB buffer and the resultant mixture was run in 1 × TB buffer at a constant voltage of 60 V for 90 min.

3. Results and discussion

3.1. Synthesis and characterization of multicore/shell CdTe@SiO_2 composite particles

The multicore/shell CdTe@SiO_2 composite particles reported herein were prepared via the reverse microemulsion method according to previous reports except that the recipe was slightly modified with more details being described in section 2. In addition, the CdTe QDs co-stabilized by thioglycerol (TG) and thioglycolic acid (TGA) prepared under optimized pH and precursor ratios exhibited a fluorescence QY of 52%, much higher than those used in previous reports [27, 28]. Rather than incubating the CdTe QDs in ammoniacal solution [34], which is a long-lasting process, poly(diallyldimethylammonium chloride) (PDDA) was introduced into the microwater droplets for reducing the electrostatic repulsion between negatively charged CdTe QDs therein to promote the multicore/shell composite structure.

Figure 1(a) shows a representative transmission electron microscopy (TEM) image of the resultant CdTe@SiO_2 composite particles. Statistical analysis on the particle ensemble reveals that approximately 80% composite particles possess multiple CdTe nanocrystal cores, slightly less than 20% particles hold single CdTe nanocrystal cores and less than 1% particles have no QDs encapsulated. On average, the number of CdTe QDs per silica sphere is estimated to be around 5 by TEM measurements through statistics and the average diameter of the CdTe@SiO_2 particles is determined to be 49 ± 7 nm. The overall particle size distribution can better been seen from the scanning electron microscopy (SEM) image shown in figure 1(b) with the particle size distribution profile being presented in figure 1(c). In general, the multicore/shell composite particles are fairly mono-dispersed, which are in favor of their further applications as biolabeling materials.

The optical properties of the resultant composite particles were further characterized by conventional electron

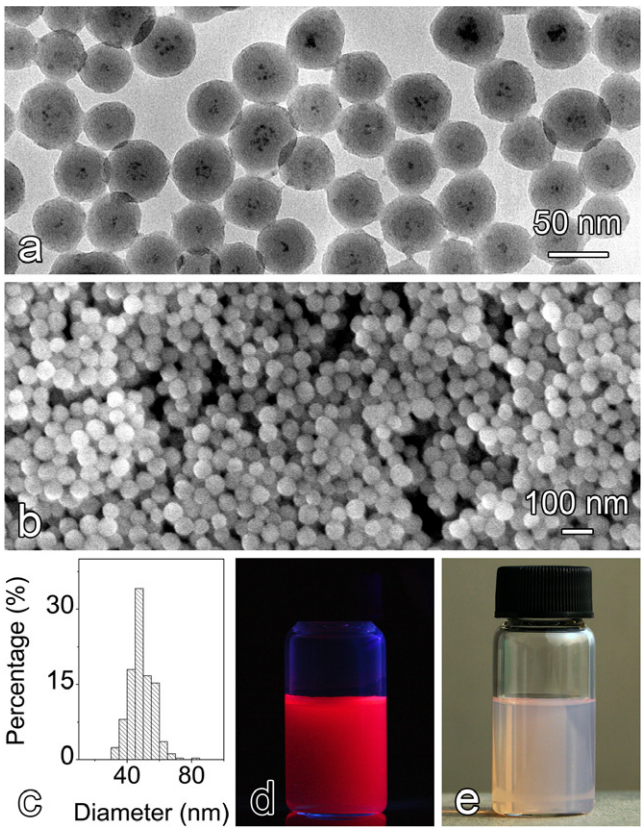

Figure 1. TEM image (a) and SEM image (b) of the as-prepared CdTe@SiO_2 composite particles together with the particle size distribution histogram (c). Panels (d) and (e) are photographs of an aqueous dispersion of the as-prepared CdTe@SiO_2 composite particles taken under UV light (d) and ambient light (e), respectively.

spectroscopy and the results are shown in figure 2. In brief, the first excitonic transition of the CdTe QDs encapsulated can still be identified in spite of the light scattering background introduced by the composite particles. Most importantly, the optical emission profile of the encapsulated CdTe QDs remains nearly unchanged in comparison with that of the mother CdTe QDs, which implies that the QDs are well electronically isolated from each other although some of them occur closely within the silica spheres as shown in figure 1(a) [43]. The room temperature fluorescence QY of the CdTe@SiO_2 composite particles was determined to be 32% according to the reference method [34], rather comparable with the fluorescence QY reported for silica particles incorporated with hydrophobic core/shell/shell QDs [29]. The high fluorescence QY makes the fluorescence of CdTe@SiO_2 composite particles visible not only under UV irradiation (figure 1(d)) but also under ambient light (figure 1(e)). In fact, the fluorescence brightness of the current sample appears rather comparable with the previously reported CdTe@SiO_2 particles with fluorescence QY up to 47%, due to the increased number of CdTe cores [34].

The optical and colloidal stability of the fluorescent particles in different chemical environments are also very important prerequisites for their applications in biolabeling and biosensing [14, 44, 45]. Therefore, the fluorescence pH dependence and the photostability of the multicore/shell CdTe@SiO_2 particles were investigated by comparing with

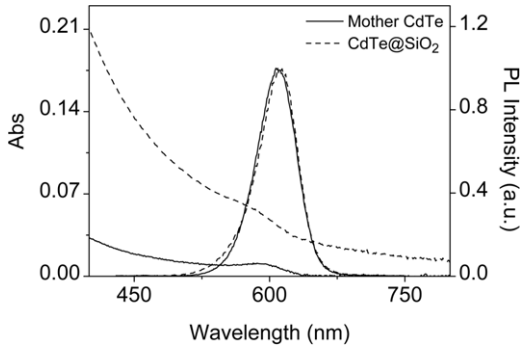

Figure 2. Absorption and normalized fluorescence spectra of mother CdTe QD and multicore/shell CdTe@SiO_2 composite particles.

the mother CdTe QDs. The results shown in figure 3(a) demonstrate that the silica coating can greatly suppress the pH-dependent behavior of the fluorescence of the mother QDs, leading to a more stable optical emission in a broad pH range from 13 down to 4, and even maintaining ~67% of the initial fluorescence intensity at pH 3 where the fluorescence of the mother QDs is completely quenched. Another reasonable expectation for silica coating of QDs is to suppress the photodegradation caused by environmental oxygen [18]. To verify the effectiveness of the silica layer in impeding oxygen diffusion, the temporal fluorescence stability of CdTe@SiO_2 composite particles dispersed in O_2-aerated aqueous solution was measured under prolonged UV irradiation and then compared with that of the mother CdTe QDs. The results presented in figure 3(b) demonstrate that the silica coating can effectively enhance the photostability of the CdTe QDs encapsulated and especially the fluorescence intensity remains nearly constant within the first 3 h of UV irradiation. In contrast, that of the mother CdTe QDs decreases by 21% within the same period of time. Moreover, the composite particles retains more than 50% of the initial fluorescence after that of the mother CdTe QDs is completely quenched after 24 h. Apart from robustness against pH and UV irradiation, the colloidal stability of the composite particles in physiological buffers is also one of the most important prerequisites for cell labeling and even *in vivo* applications [46]. Therefore, several commonly used physiological buffers were chosen to test the colloidal stability by measuring the temporal fluorescence of the multicore/shell CdTe@SiO_2 composite particles. The results shown in figure 3(c) suggest that the composite particles are very stable in PBS and DMEM. Although the fluorescence intensity slightly drops in MEM and RPMI 1640 during the initial 4 h of incubation, it remains nearly unchanged thereafter for 50 h.

3.2. Particle surface PEG coating and carboxyl derivatization

As aforementioned that suitable surface modification is required for minimizing the nonspecific adsorption of biomolecules due to the multiple surface binding sites of nanoparticle materials, while surface derivatization of reactive moieties is an effective measure for producing robust target-specific molecular probes based on covalent conjugation between nanoparticles and bioligands [37, 38, 47]. In the

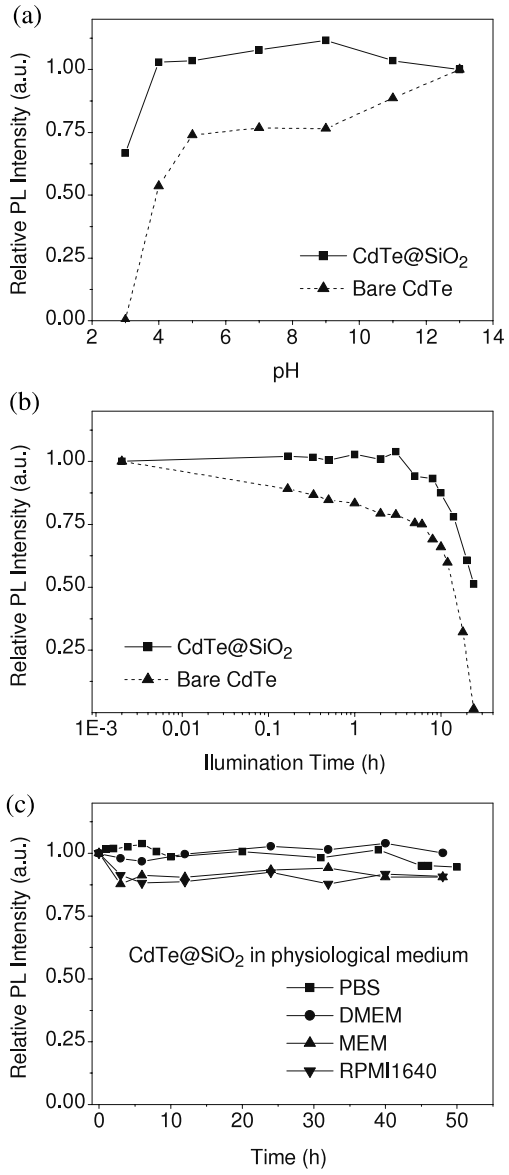

Figure 3. (a) Fluorescence of the multicore/shell CdTe@SiO_2 composite particles together with the mother CdTe QDs determined at different pH; (b) photostability of the multicore/shell CdTe@SiO_2 composite particles together with the mother CdTe QDs suspended in O_2-aerated solutions measured under prolonged UV irradiation (the power density of UV light of 292 nm was about 1.2 W cm^{-2}) and (c) colloidal stability characterized by the fluorescence fluctuation of the multicore/shell CdTe@SiO_2 particles suspended in different types of buffers. The excitation was 360 nm for all fluorescence measurements.

current study, PEG was chosen for forming the anti-biofouling coating layer for the CdTe@SiO_2 composite particles as PEG is a widely used biocompatible polymer known to have good resistance to the nonspecific bindings, while carboxyl groups were grafted on the particle surface for the further covalently attaching bioligands, which were realized through the reactions of the silanol-terminated composite particles with CES (carboxyethylsilanetriol sodium) and PEOS (methoxy(polyethyleneoxy)propyltrimethoxysilane). Different feeding molar ratios of CdTe@SiO_2:CES:PEOS were adopted, i.e. 1:0:0 (sample **A**), 1:264 000:143 250 (sample **B**), 1:66 000:143 250 (sample **C**) and 1:66 000:35 813 (sample **D**) (Note that sample **A** is herein a control for samples **B**–**D**, it was obtained after being treated exactly the same way but in the absence of CES and PEOS.) These recipes were designed in a way that the feeding amount of PEG segments on samples **B** and **C** is the same but reduced by a factor of 4 for sample **D**, while the feeding amount of carboxyl groups on samples **C** and **D** is the same but only a quarter of that on sample **B**.

The surface modification was further investigated by both hydrodynamic size and zeta potential measurements and the detailed results are provided in table 1. The hydrodynamic size profiles of samples **A**–**D** are shown in figure S1 in supplementary data (SD) (available at stacks.iop.org/Nano/22/505104/mmedia). In comparison with sample **A**, the particle size distribution of samples **B**–**D** remains nearly unchanged after the reactions with CES and PEOS, irrespective of the feeding molar ratio, which suggests that the surface reactions lead to neither agglomeration of the composite particles nor secondary nucleation. However, the surface PEG coating and carboxyl derivatization slightly decrease the hydrodynamic sizes of samples **B**–**D** though the surface-modified PEG molecules are expected to increase the physical size of the particles. The decrease in hydrodynamic size is probably caused by the fact that PEG can reduce both the particle surface charge density and the thickness of the electrical double layer. Because the PEG segment in PEOS is rather short and contains only 6–9 repeating units of C_2H_4O, the size increment by PEG coating is consequently compensated in aqueous media. The zeta potential results shown in table 1 reveal that the zeta potential of sample **B** is greatly reduced, which implies that the carboxyl groups are successfully grafted on the particle surface. The nearly unchanged zeta potential of samples **C** and **D** does not necessarily deny the carboxyl derivatization as the amount of CES used for preparing these two samples is greatly reduced in comparison with that for sample **B**. In brief, the DLS and zeta potential results imply that the surface PEG coating and carboxyl derivatization are successfully achieved. Even though it is difficult to accurately determine the exact amount of these groups, the effects of these surface modifications are quite obvious as shown below.

3.3. Conjugation of IgG to CdTe@SiO_2 composite particles

In the following preparation of molecular probes, GaHIgG was chosen to covalently conjugate to the composite particles via the amidation reaction through the particle surface carboxyl residues, in the meantime as a model protein for investigating the nonspecific interactions between IgG and the PEG-coated composite particles. The experiments were carried out in a way that the composite particles were mixed with GaHIgG in the absence (the resultant sample denoted as **A** + GaHIgG, **B** + GaHIgG, **C** + GaHIgG and **D** + GaHIgG) or the presence of EDC/Sulfo-NHS which were used to catalyze the amidation reaction (the resultant samples were denoted as **B**–GaHIgG, **C**–GaHIgG and **D**–GaHIgG). The effectiveness of the coupling reaction and the nonspecific adsorption of IgG were evaluated by the electrophoresis method. As shown in figure 4, sample **A**

Table 1. Zeta potential and hydrodynamic size of samples **A**–**D** (s.d., standard deviation).

	Zeta potential (mV)		Size by intensity (nm)		Size by number (nm)	
	Mean	s.d.	Mean	s.d.	Mean	s.d.
Sample **A**	−59.4	0.7	97.0	1.9	59.2	2.6
Sample **B**	−46.7	0.4	75.2	0.4	42.2	1.8
Sample **C**	−59.9	1.6	83.9	0.2	53.2	1.3
Sample **D**	−59.2	0.6	81.3	1.2	49.3	2.6

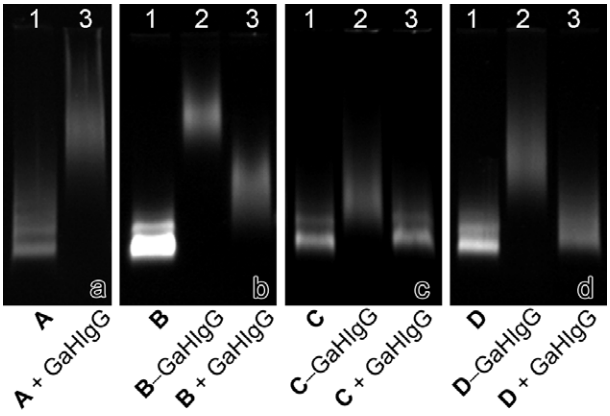

Figure 4. Gel electrophoresis images of samples **A**–**D** (line 1) together with CdTe@SiO_2–GaHIgG conjugates (**B**–GaHIgG, **C**–GaHIgG and **D**–GaHIgG) (line 2) and samples **A**–**D** obtained after being incubated with GaHIgG in the absence of EDC/Sulfo-NHS, denoted as **A** + GaHIgG, **B** + GaHIgG, **C** + GaHIgG and **D** + GaHIgG, respectively (line 3).

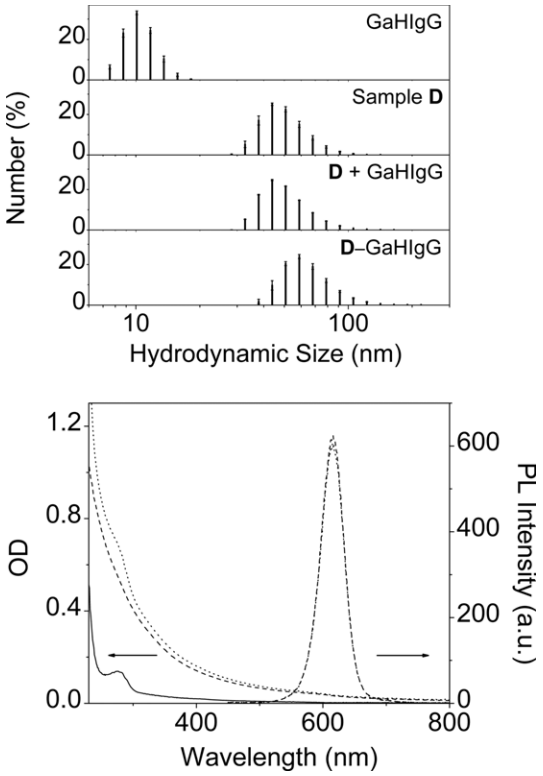

Figure 5. Upper panel: hydrodynamic size distribution profiles of GaHIgG, Sample **D**, purified sample **D** obtained after being incubated with GaHIgG (**D** + GaHIgG) and **D**–GaHIgG conjugates; lower panel: absorption and fluorescence spectra of sample **D** before (dashed line) and after (dotted line) covalently conjugated to GaHIgG. The difference absorption spectrum is shown as a solid line.

presents the strongest nonspecific interactions, with GaHIgG among all these four samples, indicated by its greatly reduced electrophoretic mobility in comparison with that of samples **C**–**D** shown in lane 3 in each panel. This is because the composite particles in sample **A** are negatively charged at pH 7.4, while GaHIgG is slightly positively charged because its isoelectric point (8.1) is slightly higher than the pH value of the incubation buffer, which inevitably leads to electrostatic attractions between them [48]. Even though samples **B**–**D** are also negatively charged (table 1), the bio-antifouling function of the PEG coating takes effect as indicated by the reduced difference between lane 1 and lane 3 in panels (b)–(d) of figure 4. The difference between lanes 1 and 2 in panels (b)–(d) however indicates the effectiveness of the coupling reaction. Therefore, it can be concluded that GaHIgG can effectively be coupled to samples **B**–**D**. But sample **B** still shows nonspecific interactions with GaHIgG in contrast to sample **C** and sample **D**, it was excluded in the following experiments. In comparison with **C**–GaHIgG, the electrophoretic band of **D**–GaHIgG exhibits nearly no overlap with that of the mother composite particles shown in panel (d) of figure 4, suggesting that GaHIgG was most effectively conjugated to sample **D** in comparison with samples **B** and **C**.

To further verify the success of the conjugation reaction and the minimization of the nonspecific adsorption of GaHIgG on the PEG-coated composite particles, DLS experiments were carried out to determine the variation in hydrodynamic size of the composite particles in sample **D** after they were simply mixed with GaHIgG or covalently conjugated to GaHIgG. The results are shown in the upper panel of figure 5 with sample **D** and GaHIgG acting as references. It is quite obvious that mixing GaHIgG with sample **D** leads to nearly no change to the size distribution profile of sample **D** after purification, suggesting that the PEG-coating layer endows the composite particles with enough resistance to the nonspecific adsorption of IgG. In contrast, the hydrodynamic size of the composite particles obtained after the conjugation reaction is increased by 17 nm in comparison with the mother particles. Taking the average hydrodynamic size of 10 nm for GaHIgG into consideration, the reasonable size increment for **D**–GaHIgG conjugates strongly supports that covalent conjugation is realized. Most importantly, the conjugation reaction does not lead to any unwanted agglomeration of the composite particles since neither do additional light scattering peaks of larger

particles appear, nor is any broadening in size distribution profile presented.

The spectroscopy results presented in the lower panel of figure 5 demonstrate that the conjugation reaction did not alter either the fluorescence intensity or the emission profile of the composite particles. Moreover, the presence of characteristic absorption of IgG at 280 nm in the absorption spectrum of the resultant conjugates—better seen from the difference spectrum—also supports the successful conjugation reaction.

3.4. Immunofluorescence labeling of cancer cells

With respect to cancer cell detection, both direct fluorescent antibody (DFA) and indirect fluorescent antibody (IFA) assays were adopted for labeling the UM-SCC-22B human head and neck squamous cell carcinoma cell line via the cell-surface-expressed EGFR which is an important cancer-related receptor not only meaningful for cancer detection but also for cancer treatment [49, 50]. DFA relies on the direct recognition of fluorescence-labeled primary antibody to antigen, while IFA relies on the recognition of a fluorescence-labeled secondary antibody to the primary antibodies pre-combined with antigen. In comparison with DFA, IFA allows for a significant fluorescence signal amplification in spite of the multi-step procedures and enhanced nonspecific signals. Moreover, IFA is technically meaningful for developing immunoassay methods. Therefore, the IFA results are mainly discussed below.

In the IFA process, anti-EGFR-mAb was incubated with UM-SCC-22B cells to bind with EGFR expressed on the cell surface. Then the resultant cells were incubated with **D**–GaHIgG conjugates with the mother sample **D** served as control. An additional control experiment was also carried out by directly incubating **D**–GaHIgG conjugates with UM-SCC-22B cells that were not treated by anti-EGFR-mAb. The detailed results are shown in figure 6. It is quite obvious that the cancer cells can effectively be stained by the **D**–GaHIgG conjugates after the cell surface EGFR is pre-combined with anti-EGFR-mAb (row (a) of figure 6). A comparison of the fluorescence image (left) with the differential interference contrast image (middle) reveals that the fluorescence is mainly from the cell membrane, suggesting that the cancer cells are successfully labeled by the fluorescent nanoprobes via the specific secondary antibody—primary antibody interaction. However, a certain degree of background noise is also presented in the fluorescence image shown in row (a). Careful experimental observations suggest that the background noise comes from the cell fragments labeled by **D**–GaHIgG. Such cell fragments was observed from the cell samples prior to the labeling process as shown in figure S2 in SD (available at stacks.iop.org/Nano/22/505104/mmedia). Owing to the fast proliferation feature of the UM-SCC-22B cells, the cell fragments carrying EGFR were inevitably formed while plating the cells on the glass bottom of confocal dishes overnight. Nevertheless, such fragments are not stained with respect to the sample shown in row (b), which strongly supports that **D**–GaHIgG possesses satisfying binding specificity. Quite comparable results based on the DFA approach were also obtained by directly targeting

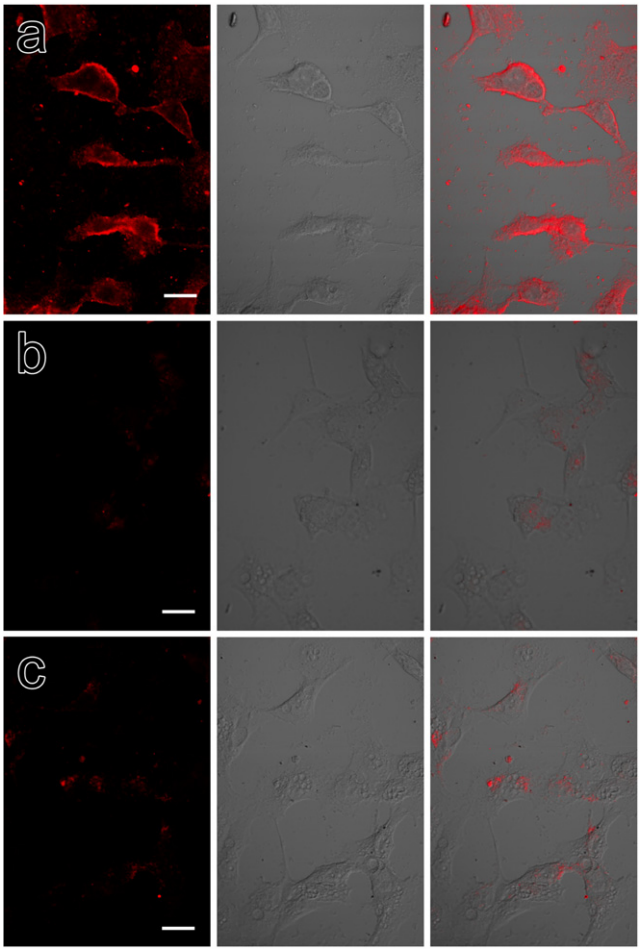

Figure 6. Confocal fluorescence images (left), differential interference contrast images (middle) and their merged images (right) of the fixed UM-SCC-22B cells labeled by **D**–GaHIgG conjugates (rows (a) and (b)) or the mother CdTe@SiO_2 particles in sample **D** (row (c)). (Note that the cancer cells shown in rows (a) and (c) were pre-treated with anti-EGFR-mAb in contrast to those shown in row (b).) The scale bars in all micrographs correspond to 25 μm.

the cell-surface-expressed EGFR using **D**–(anti-EGFR-mAb) conjugates (figures S3 and S4 in SD (available at stacks.iop.org/Nano/22/505104/mmedia)). In contrast, the cancer cells that were not treated by anti-EGFR-mAb show very weak fluorescence after being incubated with **D**–GaHIgG (Row (b) of figure 6), quite comparable to the cells treated by anti-EGFR-mAb but stained by the mother sample **D** (row (c) of figure 6), which suggests that the weak staining of the cancer cells by **D**–GaHIgG probes, observed in the absence of anti-EGFR-mAb, is quite probably caused by the nonspecific binding inherited from the mother composite particles. In brief, the above results clearly demonstrate that the currently reported PEG anti-biofouling coating and the following bioconjugation via the particle surface carboxyl residues are generally very effective for producing CdTe@SiO_2-based molecular probes showing excellent binding specificity to the EGFR target, but they do not represent the best optimization yet.

4. Conclusions

In summary, multicore/shell CdTe@SiO_2 composite particles of ∼50 nm are successfully prepared by the reverse microemulsion method upon the hydrolysis of TEOS in the confined water microdroplets. The CdTe QDs encapsulated in the silica matrix exhibit a fluorescence QY of 32%. Consequently, the resultant composite particles present very bright fluorescence even under ambient light due to the multicore/shell structure. Towards cancer cell detection, PEG segments and carboxyl moieties are further modified on the composite particle surface, on the one hand to minimize the nonspecific interactions with cells, and on the other hand to conjugate bioligands of interest for forming molecular nanoprobes. Under optimized conditions, the PEG-coated CdTe@SiO_2 composite particles present satisfying resistance to IgG adsorption, which enables the following fluorescence staining of cancer cells by using the composite particle-based molecular probes. Cancer cell labeling experiments demonstrate that both CdTe@SiO_2–GaHIgG and CdTe@SiO_2–(anti-EGFR-mAb) covalent conjugates present excellent binding specificity in detecting the UM-SCC-22B human head and neck squamous cell carcinoma cell line through the IFA and DFA approaches, respectively. Different from previously published silica-coated QDs, the current composite particles are characterized by a much thick silica coating layer which provides the resultant composite particles excellent colloidal stability under physiological conditions and remarkable robustness against photobleaching. Moreover, the simultaneous surface PEG modification and carboxyl derivatization provide the composite particles with satisfying anti-biofouling surface and biofunctionality. Therefore, the resultant particles are not solely limited by the cell labeling applications and also hold promise for many other biological and biomedical applications.

Acknowledgments

The current study was jointly supported by the National Basic Research Program of China (2011CB935800) and NSFC projects (81090271, 21003135 and 20820102035), the 863 project (2010AA06Z302) and the Croucher Foundation project (9220054). JLH acknowledges Mr Xujie Liu at Peking University for technical help with the UM-SCC-22B cell line.

References

[1] Alivisatos A P 2004 *Nature Biotechnol.* **22** 47–52
[2] Michalet X, Pinaud F F, Bentolila L A, Tsay J M, Doose S, Li J J, Sundaresan G, Wu A M, Gambhir S S and Weiss S 2005 *Science* **307** 538–44
[3] Medintz I L, Uyeda H T, Goldman E R and Mattoussi H 2005 *Nature Mater.* **4** 435–46
[4] Gill R, Zayats M and Willner I 2008 *Angew. Chem. Int. Edn* **47** 7602–25
[5] Wang S P, Mamedova N, Kotov N A, Chen W and Studer J 2002 *Nano Lett.* **2** 817–22
[6] Somers R C, Bawendi M G and Nocera D G 2007 *Chem. Soc. Rev.* **36** 579–91
[7] Hu F Q, Ran Y L, Zhou Z A and Gao M Y 2006 *Nanotechnology* **17** 2972–7
[8] Biju V, Itoh T and Ishikawa M 2010 *Chem. Soc. Rev.* **39** 3031–56
[9] Dubertret B, Skourides P, Norris D J, Noireaux V, Brivanlou A H and Libchaber A 2002 *Science* **298** 1759–62
[10] Kim S *et al* 2004 *Nature Biotechnol.* **22** 93–7
[11] Li Y L, Duan X, Jing L H, Yang C H, Qiao R R and Gao M Y 2011 *Biomaterials* **32** 1923–31
[12] Rogach A L (ed) 2008 *Semiconductor Nanocrystal Quantum Dots: Synthesis, Assembly, Spectroscopy* (New York: Springer)
[13] Nazzal A Y, Wang X Y, Qu L H, Yu W, Wang Y J, Peng X G and Xiao M 2004 *J. Phys. Chem.* B **108** 5507–15
[14] Boldt K, Bruns O T, Gaponik N and Eychmüller A 2006 *J. Phys. Chem.* B **110** 1959–63
[15] Kloepfer J A, Bradforth S E and Nadeau J L 2005 *J. Phys. Chem.* B **109** 9996–10003
[16] Derfus A M, Chan W C W and Bhatia S N 2004 *Nano Lett.* **4** 11–8
[17] Han M Y, Gao X H, Su J Z and Nie S 2001 *Nature Biotechnol.* **19** 631–5
[18] Correa-Duarte M A, Giersig M and Liz-Marzán L M 1998 *Chem. Phys. Lett.* **286** 497–501
[19] Parak W J *et al* 2002 *Chem. Mater.* **14** 2113–9
[20] Gerion D, Pinaud F, Williams S C, Parak W J, Zanchet D, Weiss S and Alivisatos A P 2001 *J. Phys. Chem.* B **105** 8861–71
[21] Rogach A L, Nagesha D, Ostrander J W, Giersig M and Kotov N A 2000 *Chem. Mater.* **12** 2676–85
[22] Selvan S T, Tan T T and Ying J Y 2005 *Adv. Mater.* **17** 1620–5
[23] Nann T and Mulvaney P 2004 *Angew. Chem. Int. Edn.* **43** 5393–6
[24] Gao X H, Cui Y Y, Levenson R M, Chung L W K and Nie S M 2004 *Nature Biotechnol.* **22** 969–76
[25] Chan Y, Zimmer J P, Stroh M, Steckel J S, Jain R K and Bawendi M G 2004 *Adv. Mater.* **16** 2092–7
[26] Darbandi M, Thomann R and Nann T 2005 *Chem. Mater.* **17** 5720–5
[27] Yang Y H and Gao M Y 2005 *Adv. Mater.* **17** 2354–7
[28] Yang Y H, Jing L H, Yu X L, Yan D D and Gao M Y 2007 *Chem. Mater.* **19** 4123–8
[29] Koole R, van Schooneveld M M, Hilhorst J, Donega C D, 't Hart D C, van Blaaderen A, Vanmaekelbergh D and Meijerink A 2008 *Chem. Mater.* **20** 2503–12
[30] Yang P and Murase N 2010 *ChemPhysChem* **11** 815–21
[31] Zhelev Z, Ohba H and Bakalova R 2006 *J. Am. Chem. Soc.* **128** 6324–5
[32] Guerrero-Martinez A, Perez-Juste J and Liz-Marzán L M 2010 *Adv. Mater.* **22** 1182–95
[33] Kumar R, Ding H, Hu R, Yong K T, Roy I, Bergey E J and Prasad P N 2010 *Chem. Mater.* **22** 2261–7
[34] Jing L H, Yang C H, Qiao R R, Niu M, Du M H, Wang D Y and Gao M Y 2010 *Chem. Mater.* **22** 420–7
[35] Choi H S, Liu W H, Liu F B, Nasr K, Misra P, Bawendi M G and Frangioni J V 2010 *Nature Nanotechnol.* **5** 42–7
[36] Pinaud F, Clarke S, Sittner A and Dahan M 2010 *Nature Methods* **7** 275–85
[37] Bentzen E L, Tomlinson I D, Mason J, Gresch P, Warnement M R, Wright D, Sanders-Bush E, Blakely R and Rosenthal S J 2005 *Bioconjug. Chem.* **16** 1488–94
[38] Liu W, Howarth M, Greytak A B, Zheng Y, Nocera D G, Ting A Y and Bawendi M G 2008 *J. Am. Chem. Soc.* **130** 1274–84
[39] Gao M Y, Kirstein S, Möhwald H, Rogach A L, Kornowski A, Eychmüller A and Weller H 1998 *J. Phys. Chem.* B **102** 8360–3

[40] Gong Y J, Gao M Y, Wang D Y and Möhwald H 2005 *Chem. Mater.* **17** 2648–53
[41] Shavel A, Gaponik N and Eychmüller A 2006 *J. Phys. Chem.* B **110** 19280–4
[42] Rogach A L, Franzl T, Klar T A, Feldmann J, Gaponik N, Lesnyak V, Shavel A, Eychmüller A, Rakovich Y P and Donegan J F 2007 *J. Phys. Chem.* C **111** 14628–37
[43] Kagan C R, Murray C B and Bawendi M G 1996 *Phys. Rev.* B **54** 8633–43
[44] Stewart M H, Susumu K, Mei B C, Medintz I L, Delehanty J B, Blanco-Canosa J B, Dawson P E and Mattoussi H 2010 *J. Am. Chem. Soc.* **132** 9804–13
[45] Hu X G and Gao X H 2010 *ACS Nano* **4** 6080–6
[46] Qiao R R, Yang C H and Gao M Y 2009 *J. Mater. Chem.* **19** 6274–93
[47] Howarth M, Liu W H, Puthenveetil S, Zheng Y, Marshall L F, Schmidt M M, Wittrup K D, Bawendi M G and Ting A Y 2008 *Nature Methods* **5** 397–9
[48] Liu S J, Han Y C, Qiao R R, Zeng J F, Jia Q J, Wang Y L and Gao M Y 2010 *J. Phys. Chem.* C **114** 21270–6
[49] Yang L L *et al* 2009 *Small* **5** 235–43
[50] El-Sayed I H, Huang X H and El-Sayed M A 2005 *Nano Lett.* **5** 829–34